Linking Siberian Snow Cover to Precursors of Stratospheric Variability

Citation: Cohen, Judah, Jason C. Furtado, Justin Jones, Mathew Barlow, David Whittleston, and Dara Entekhabi. "Linking Siberian Snow Cover to Precursors of Stratospheric Variability." J. Climate 27, no. 14 (July 2014): 5422–5432. © 2014 American Meteorological Society.

As Published: http://dx.doi.org/10.1175/JCLI-D-13-00779.1

Publisher: American Meteorological Society

Persistent URL: http://hdl.handle.net/1721.1/93892

Version: Final published version: final published article, as it appeared in a journal, conference proceedings, or other formally published context

Linking Siberian Snow Cover to Precursors of Stratospheric Variability

JUDAH COHEN, JASON C. FURTADO, AND JUSTIN JONES

Atmospheric and Environmental Research, Lexington, Massachusetts

MATHEW BARLOW

Environmental, Earth, and Atmospheric Sciences, University of Massachusetts Lowell, Lowell, Massachusetts

DAVID WHITTLESTON AND DARA ENTEKHABI

Department of Civil and Environmental Engineering, Massachusetts Institute of Technology, Cambridge, Massachusetts

(Manuscript received 17 December 2013, in final form 31 March 2014)

ABSTRACT

Previous research has linked wintertime Arctic Oscillation (AO) variability to indices of Siberian snow cover and upward wave activity flux in the preceding fall season. Here, daily data are used to examine the surface and tropospheric processes that occur as the link between snow cover and upward forcing into the stratosphere develops. October Eurasian mean snow cover is found to be significantly related to sea level pressure (SLP) and to lower-stratosphere (100 hPa) meridional heat flux. Analysis of daily SLP and 100-hPa heat flux shows that in years with high October snow, the SLP is significantly higher from approximately 1 November to 15 December, and the 100-hPa heat flux is significantly increased with a two-week lag, from approximately 15 November to 31 December. During November–December, there are periods with upward wave activity flux extending coherently from the surface to the stratosphere, and these events occur nearly twice as often in high snow years compared to low snow years. The vertical structure of these events is a westward-tilting pattern of high eddy heights, with the largest normalized anomalies near the surface in the same region as the snow and SLP changes. These results suggest that high SLP develops in response to the snow cover and this higher pressure, in turn, provides part of the structure of a surface-to-stratosphere wave activity flux event, thus making full events more likely. Implications for improved winter forecasts exist through recognition of these precursor signals.

1. Introduction

Over the last few decades there has been significant progress in our ability to predict tropical climate variability on seasonal time scales based on the ocean–atmosphere coupling associated with the El Niño–Southern Oscillation (ENSO; Rasmusson and Carpenter 1982; Kim et al. 2012) and intraseasonal time scales based on the Madden–Julian oscillation (MJO; Madden and Julian 1994). The same rate of progress in predictive skill and even in basic understanding is not evident for extratropical climates especially in the winter season (Quan et al. 2006; Delsole and Shukla 2006; Saha et al. 2006; Kumar et al. 2007; Cohen and Jones 2011a; Kim et al. 2012). Understanding the mechanisms of winter climate variability sufficiently well to produce consistently accurate winter climate predictions on intraseasonal-to-seasonal time scales would not only provide benefit for all those with exposure to shorter-term weather risk, but would also increase the public's confidence in longer-term projections related to climate change.

The Arctic Oscillation (AO) is the dominant mode of atmospheric winter climate variability in the extratropics (Thompson and Wallace 1998, 2001). The AO is the first empirical orthogonal function of sea level pressure (SLP) poleward of 20°N and is a measure of the meridional vacillations in the polar jet stream that consequently governs temperatures and precipitation patterns in the extratropical NH. Therefore, successfully predicting the winter AO is considered the most important

Corresponding author address: Judah Cohen, Atmospheric and Environmental Research, 131 Hartwell Ave., Lexington, MA 02421. E-mail: jcohen@aer.com

DOI: 10.1175/JCLI-D-13-00779.1

advance in winter seasonal prediction (Cohen and Jones 2011a).

Seasonal predictability of the AO remains a challenge as it is considered unpredictable beyond a week or so (Feldstein 2002) and may in part explain why prediction models on intraseasonal-to-seasonal time scales have large errors. However, recent studies suggest enhanced predictability of the tropospheric AO is possible through monitoring changes in more slowly varying boundary conditions. Variability in the extratropical stratospheric circulation has been shown to lead variability in the troposphere, with the same-signed phase of the AO favored for up to two months in the troposphere following a strong stratospheric AO event (e.g., Baldwin and Dunkerton 2001; Christiansen 2005). Furthermore, internal variability of the wintertime extratropical stratosphere is ultimately forced by upward-propagating tropospheric waves generated through either topography or preferential synoptic-scale patterns (Charney and Drazin 1961; Matsuno 1970). Seasonal variability in the AO also has relationships with Arctic sea ice variability (e.g., Liu et al. 2004, 2012; Honda et al. 2009), ENSO (Ineson and Scaife 2009; Garfinkel et al. 2010), North Atlantic sea surface temperatures (Keeley et al. 2009; Folland et al. 2012), the quasi-biennial oscillation (QBO; Pascoe et al. 2006), volcanic eruptions (Stenchikov et al. 2006; Marshall et al. 2009), and stratospheric water vapor (Joshi et al. 2006).

Our focus is on the possible dynamical relationship between October snow cover extent (SCE) and the boreal winter AO as first demonstrated in Cohen and Entekhabi (1999). Cohen and Jones (2011a) developed a new index not based on the monthly extent of snow cover but rather on the rate of advance of snow cover south of 60°N that is even more highly correlated with the winter AO ($r \sim 0.8$) referred to as the snow advance index (SAI). Using reanalysis datasets, Peings et al. (2013) corroborated the high correlation between the SAI and the winter AO since the 1970s but earlier in the century they found the correlation to be much lower and, therefore, they argue that the relationship is nonstationary. They suggest that changes in the QBO between the two time periods may explain the change in the snow–AO relationship. Another explanation for the change in the snow–AO relationship could be related to the climate shift around 1976 (Christiansen 2003). These potential multidecadal changes in the relationship between fall snow cover and the winter AO require further study.

Even though the dynamical models cannot accurately predict the phase and amplitude of the AO (Cohen et al. 2005; Hoskins 2013), or the observed relationship between fall snow cover and the winter AO (e.g., Hardiman et al. 2008) possibly due to problems capturing the observed climatological stationary wave pattern (Smith et al. 2011), still a few climate models forced with prescribed snow cover have simulated the AO response to snow cover anomalies similar to what is observed, especially when forced with realistic snow cover (Allen and Zender 2011) and stratospheric variability (Peings et al. 2012).

Applying the demonstrated relationship between autumn SCE and the winter AO, a statistical model that uses October SCE and autumn NH SLP patterns as the two main predictors has been developed and shown to outperform most dynamical models in both hindcasts and forecasts of NH winter surface temperatures (Cohen and Fletcher 2007). Cohen et al. (2007) propose a chain of events by which the variability of Eurasian snow cover in October forces the phase of the winter AO: the rapid (slow) advance of snow cover leads to a strengthened (weakened) Siberian high, an increased (decreased) poleward heat flux, polar stratospheric warming (cooling), downward propagation of the associated circulation anomalies, and a negative (positive) AO in the lower troposphere. This snow–AO cycle can be summarized as a troposphere–stratosphere–troposphere coupling. More broadly, the troposphere–stratosphere part can be thought of as the vertical wave activity flux over the region being sensitive to surface conditions during a climatologically sensitive period.

The downward part of this mechanism, the stratosphere–troposphere coupling component, has been previously analyzed (see Cohen et al. 2007) and has been shown to be coherent in time. However, the space–time evolution of the initial upward part of this mechanism, the troposphere–stratosphere coupling component where snow cover variability forces a Siberian high response and subsequently impacts the poleward heat flux, has not yet been considered in detail. An initial result is a modeling experiment forced with high and low snow cover (Fletcher et al. 2009), which found that the isentropes "dome" in the high snow cover experiments; based on the conservation of potential vorticity, this should produce an upstream high surface pressure center.

Part of the incomplete understanding of the mechanism that connects October snow cover variability to the stratosphere is the issue of the time delay between the snow cover forcing in October and the atmospheric response in December and January. Smith et al. (2011) argue that the Rossby wave train associated with October snow cover variability does not constructively interfere with the climatological wave until December. However, they do not show how the signal persists from October to December and where the signal resides.

Here we focus on the upward part of the proposed troposphere–stratosphere–troposphere relationship, using

daily data to examine the spatial evolution of the atmospheric response to snow cover and the subsequent development of wave activity flux throughout the troposphere and into the stratosphere. We first document the development of the lagged relationships between snow cover, sea level pressures, and heat flux into the lower stratosphere and then examine the vertical structure of the wave activity flux anomalies that link the surface changes to the heat flux entering the stratosphere.

2. Data and methods

Observational atmospheric data originate from the National Aeronautics and Space Administration (NASA)'s Modern-Era Retrospective Analysis for Research and Applications (MERRA; Rienecker et al. 2011). The data are on a 1.25° × 1.25° longitude–latitude global grid and extend vertically on pressure levels up into the lower mesosphere. For our analyses, we focus on data below 10 hPa. Both daily- and monthly-mean fields are used, and anomalies are calculated by removing the long-term daily and monthly means from the fields, respectively. Primary variables for our analysis include SLP, temperature, geopotential height, and winds. The period for analysis is 1979–2011 (including atmospheric variables for winter 2011/12). SCE data are derived from the Rutgers Global Snow Laboratory. The data are a merged product of map reanalyses and satellite-derived measurements of snow cover over the Northern Hemisphere (Robinson et al. 1993). Monthly-mean SCE values are regridded onto an 89 × 89 grid. The record extends from 1967 to the present, but only values from 1979 to 2011 are considered for the study. (The data are available from Rutgers: http://climate.rutgers.edu/snowcover/index.php.) All data were detrended prior to linear analysis.

Three indices are used as reference for different composites and regressions in the paper:

1) October Eurasian SCE: The October mean Eurasian SCE index is formed by calculating the monthly-mean area of snow-covered grid points for the Eastern Hemisphere (between 0° and 180° latitude) from satellite-derived measurements (methodology described in Robinson et al. 1993) during October. We then chose the 15 highest and lowest monthly-mean snow cover extent years listed in Table 1. The years chosen were not sensitive to trends in the snow cover time series.
2) Siberian high variability: We constructed a daily time series of SLP for each grid point within a domain in central Eurasia (Fig. 1) and area weighed the SLP value to create an area-averaged mean SLP index. As such, this index reflects the strength of the Siberian high on a particular day, with higher values indicating a stronger Siberian high. We varied the domain by contracting and expanding the size of the box by 5° in each direction simultaneously and individually in each direction. Our results are insensitive to the choice of domain.
3) Meridional heat flux variability: To measure the variability of the lower stratospheric meridional heat flux over the extratropics, we calculated the anomalous daily 100-hPa meridional heat flux. The daily heat flux is calculated from the deviation from the zonal mean of the meridional component of the wind times the deviation from the zonal-mean temperature (see Fig. 6). The daily values are then time averaged for the month of December (see Fig. 4) denoted by an overbar and/or are area averaged between 40° and 80°N denoted by a bracket (see Figs. 4 and 5, respectively). Not only does this metric describe poleward heat flux, but it also represents upwelling tropospheric wave energy into the lower stratosphere (e.g., Eliassen and Palm 1961).

TABLE 1. Years used to composite for both high and low October Eurasian snow cover extent.

High snow cover years	Low snow cover years
1982	1979
1984	1980
1985	1981
1993	1983
1995	1986
1996	1987
1998	1988
1999	1989
2000	1990
2001	1991
2002	1992
2003	1994
2004	1997
2006	2007
2009	2008

Finally we test the statistical significance of the mean difference in the mean SLP and 100-hPa poleward heat flux fields between the 15 high and low snow cover years (as shown by the thicker black lines in Fig. 5) using Monte Carlo simulations with 10^7 random samples. First, 10^4 random combinations of 15 years were used to produce composites of November through February SLP and poleward heat flux signals. For each of these combinations, 50 time windows between 10 and 90 days were randomly chosen. A ''sliding window'' approach was then used 20 times (for each 15-yr composite of high and low SCE and each window length) to randomly select a period during winter (November–February) for which to calculate mean SLP or poleward heat flux. In this way, the significance test made no a priori assumption

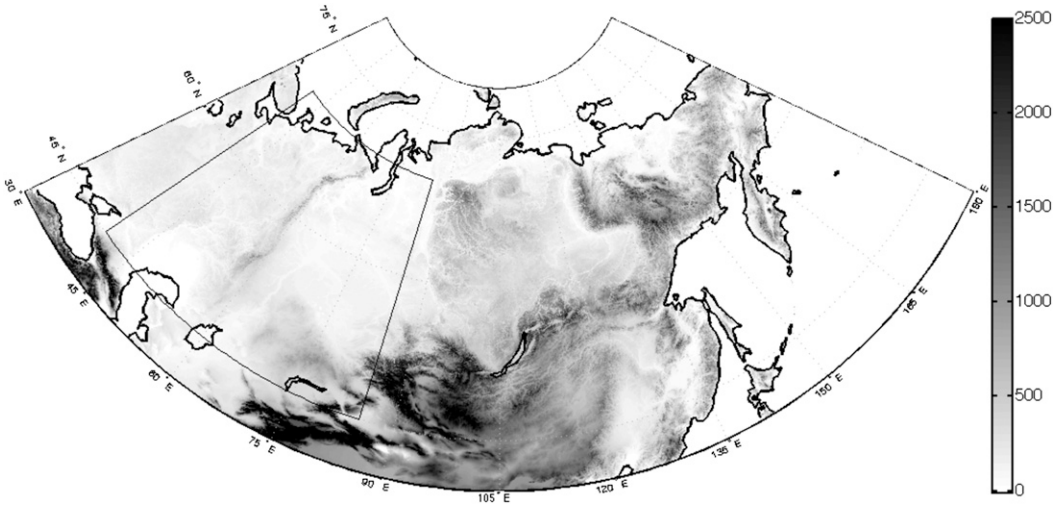

FIG. 1. Domains used to calculate snow cover extent and Siberian high strength metric. The outer domain is used to calculate October monthly-mean SCE. The inner domain was used to compute the mean SLP signals shown in Fig. 5a. The inner domain is 45°–70°N, 40°–85°E. Shading represents the orography in meters.

about when we expect an anomaly to occur and also considered anomalies of varying persistence. This approach gave 10^7 mean values that were then used to produce a cumulative distribution function.

3. Results

Through observational analysis we will show that the forcing, or at least the leading indicators, reside in the land surface boundary and the lower troposphere starting in October and can be followed through the atmosphere continuously in time until the midwinter atmospheric circulation response; therefore, completing the snow–AO loop and filling the time span from October to January for the troposphere–stratosphere–troposphere mechanism discussed in the introduction.

a. Snow cover variability

In Fig. 2 we show the monthly-mean snow cover extent for both October and November as well as the associated variance. In October the snow cover makes great advances across Eurasia mostly poleward of 60°N. The variability in October is centered on the 60th parallel and extends from around 45° to 70°N. In November the snow cover advances farther to the south and west across Eurasia mostly equatorward of 60°N. The variability in November is centered on the 45th parallel and extends from around 40° to 60°N.

b. Polar cap and troposphere–stratosphere–troposphere coupling

Figure 3 shows the correlation between October Eurasian snow cover and area-averaged geopotential height anomalies poleward of 60°N [i.e., polar cap heights (PCH)]. Similar analysis was shown in Cohen et al. (2007) and Smith et al. (2011), but an updated version is presented here. The strongest atmospheric response to snow cover variability does not occur in the autumn but rather at the end of December through mid- to late January. Also the main response does first appear in the stratosphere with the positive correlations that peak in the stratosphere in January extending all the way to the surface consistent with previous studies (Baldwin and Dunkerton 1999, 2001). Earlier there are positive correlations in the troposphere only, mostly from mid-October through the end of November. Positive correlations reflect that high snow cover is associated with positive PCH and consequently warmer Arctic temperatures, a weakened polar vortex, and the negative phase of the AO.

c. Snow and SLP link

Figure 3 suggests that heights are increased (decreased) in the high-latitude troposphere during November following high (low) Eurasian snow cover extent during October. To visualize the spatial pattern in lower-tropospheric height anomalies, Fig. 4 shows the regression of SLP anomalies onto the October Eurasian snow cover index (contours). A tripole SLP pattern emerges with positive SLP anomalies across northwest Asia and negative SLP anomalies in the North Pacific and the North Atlantic. To place this pattern in context with connections to the stratosphere, the shaded contours in Fig. 4 illustrate the regression of November SLP anomalies with the December 100-hPa meridional heat flux index. The SLP–heat flux pattern resembles a wave-2

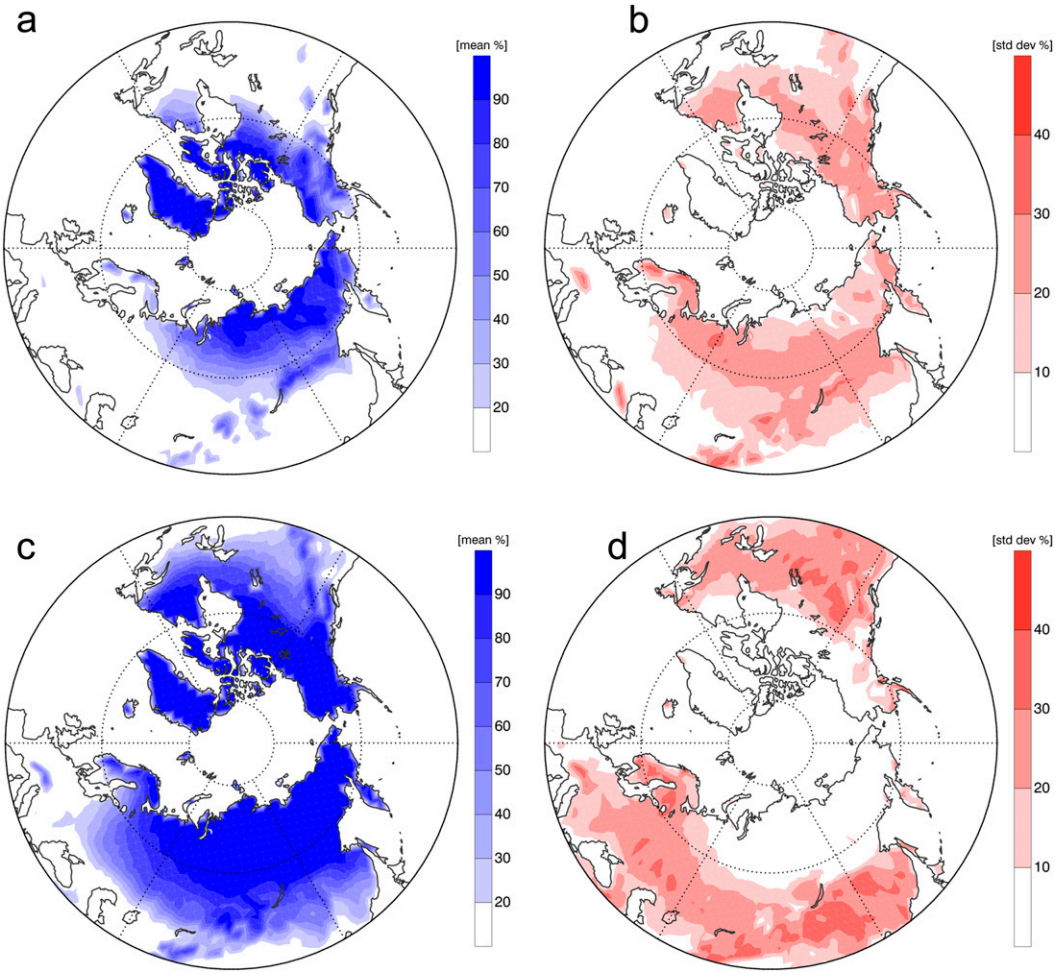

FIG. 2. (a) Mean SCE (%) for October; (b) standard deviation (%) of October SCE; and (c),(d) as in (a),(b), but for November.

SLP pattern, with anomalously strong poleward heat flux anomalies associated with low pressure anomalies in the northern ocean basins and high pressure anomalies over the northern continents, particularly with the dominant high pressure anomaly center across northwestern Eurasia. This SLP–heat flux pattern resembles the preferred tropospheric precursor pattern to major sudden stratospheric warmings (Garfinkel et al. 2010; Kolstad and Charlton-Perez 2011; Kolstad et al. 2010; Cohen and Jones 2011b). Therefore, the superposition of the line

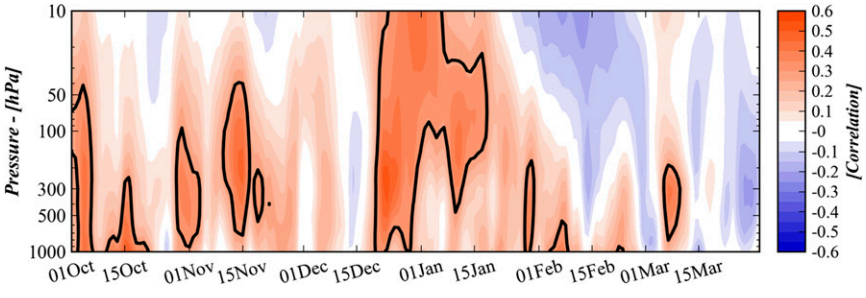

FIG. 3. Correlation of October monthly-mean Eurasian SCE and daily PCH from 1 Oct to 31 Mar. Thick black lines denote regression coefficients significant at the $p < 0.1$ level based on a two-tailed Student's t test.

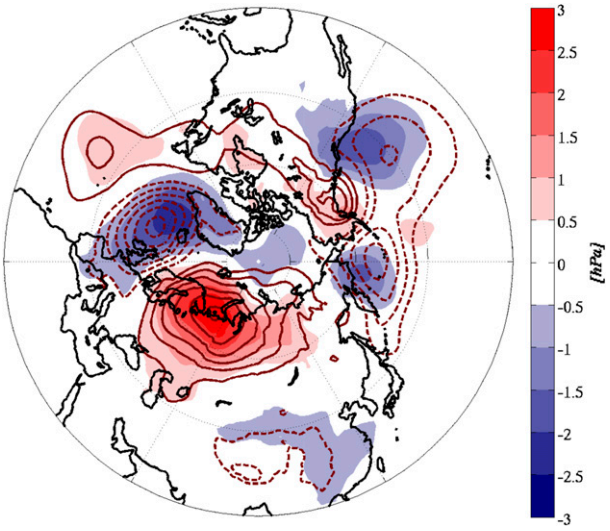

FIG. 4. Regression of November SLP anomalies (hPa) onto October monthly-mean Eurasian SCE (contouring) and onto December meridional heat flux anomalies at 100 hPa, averaged between 40° and 80°N (shading). Pattern correlation between the two regression maps (between 40° and 80°N) is 0.93.

and shaded contours in Fig. 4 suggests that the lower-tropospheric circulation anomalies constructively project onto the lower-tropospheric precursor pattern to enhanced vertical wave propagation and polar vortex disruption in the following winter. Indeed, the pattern correlation of the two regression patterns between 40° and 80°N (a key region for vertical wave propagation; see Fig. 6) is 0.93.

To further demonstrate the relationship between October snow cover variability and changes in the lower-tropospheric height fields and its persistence, we plot in Fig. 5a the composite mean Siberian high index (see section 2) for the top 15 (red curve) and bottom 15 (blue curve) years of October Eurasian SCE. Interestingly, during October, lower pressure is more prevalent in the region during high SCE years than low SCE years, likely indicating a higher frequency of synoptic low pressure systems dropping snow across the region. Once the snow cover is present, a rapid transition takes place from low to high pressure during early November. Extensive October Eurasian SCE favors more expansive high pressure in that region throughout November and the first half of December than for low October Eurasian SCE. The composite mean difference from November to early December (4.3 hPa) is significantly different based on a Monte Carlo significance test ($p < 0.05$). This significant difference in the pressure field between high and low snow cover years illustrates the importance of the Eurasian SCE in maintaining the Eurasian high pressure anomaly, which is related to lower-stratospheric poleward heat flux in early winter (e.g., Fig. 4). The initial atmospheric response to Eurasian SCE variability is the strengthening or weakening of the westward expansion of the Siberian high in the mean for a six-week period. This length of time is much longer than would be expected from synoptic-scale variability alone and in part temporally bridges the gap from October to mid-December in snow–atmosphere coupling.

d. *Snow and heat flux link*

Both the rapid advance of Eurasian snow cover and the building of high pressure across northwestern Asia have been linked with an increase in poleward heat flux that results in stratospheric warmings (Cohen et al. 2007; Cohen and Jones 2011b). In Fig. 5b, we plot the area-averaged (40°–80°N) heat flux at 100 hPa for the same high and low October Eurasian SCE years as in Fig. 5a. The zonal belt 40°–80°N is chosen for this analysis since this is the region where the highest variance in December meridional heat flux at 100 hPa occurs (Fig. 6), with an absolute maximum in variance seen over far northeast Siberia. When October Eurasian SCE is high, the mean poleward lower-stratospheric heat flux is significantly greater from mid-November through December than during low SCE years based on Monte Carlo simulations (composite mean difference is 9.9 K m s^{-1}; $p < 0.05$), illustrating that the NH stratospheric polar vortex is more likely to be disturbed in winters following high October Eurasian SCE than low October Eurasian SCE (e.g., Polvani and Waugh 2004). This weakened polar vortex would lead to higher PCH first in the stratosphere and then in the troposphere, as shown in Fig. 2. Hence, the results of Fig. 5 together with Fig. 3 present a physical basis for the continuum in time of the six-step mechanism described in Cohen et al. (2007).

Interestingly, following the initiation of the main pulses of poleward heat flux that result in a stratospheric warming, no preference is seen for high pressure over northwest Eurasia during high SCE years, likely indicating that the high pressure anomaly center shifts to the pole as expected during the negative phase of the AO. However, there does appear to be a tendency for higher pressure over Eurasia in January for low SCE years (Fig. 5a), but without a corresponding significant difference in heat fluxes during January from high SCE years (Fig. 5b).

To consider how the surface SLP signal is linked to the stratosphere, we examine the vertical structure of the height field. We consider events when two criteria are both met during November–December, based on daily data: 1) the vertical component of the wave activity flux (WAF), which is proportional to the meridional heat flux (Plumb 1985) is positive at all levels in

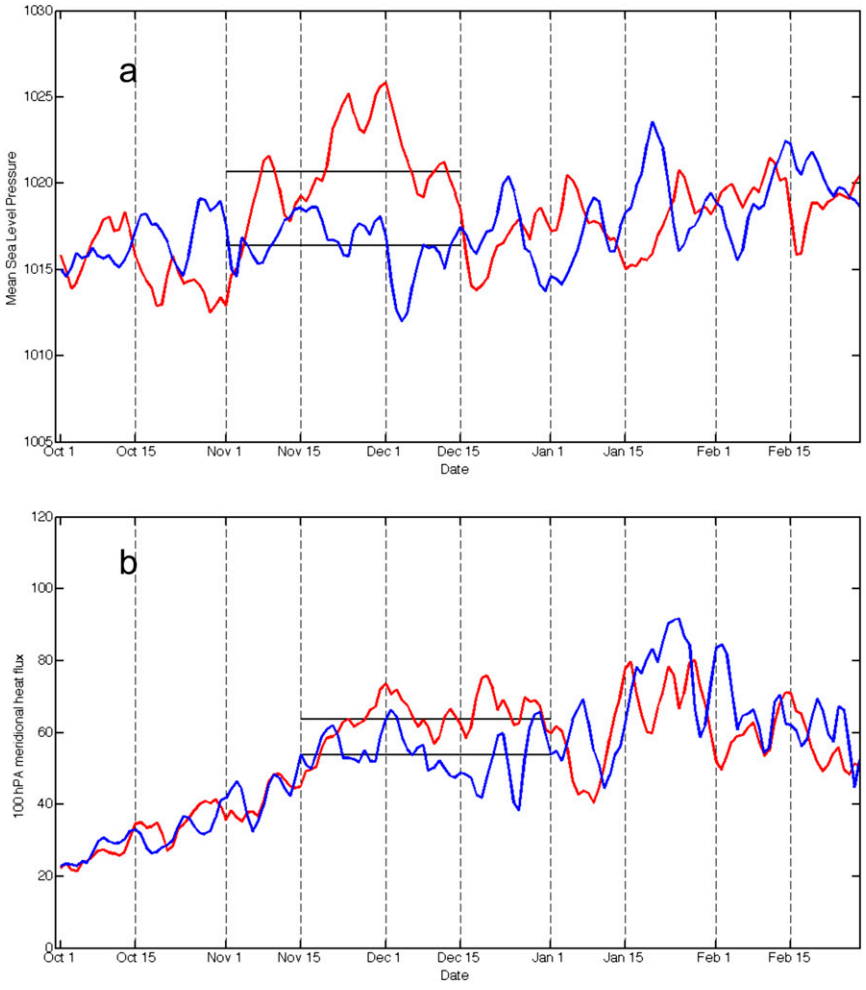

FIG. 5. (a) Mean SLP values and (b) positive heat flux events at 100 hPa for high October snow cover (red) and low October snow cover (blue) seasons from 1 Oct to 28 Feb. Also shown is the mean value from 1 Nov to 15 Dec in (a) and from 15 Nov to 31 Dec in (b) for both high and low snow cover means (black lines).

the troposphere; and 2) SLP is high, based on the Siberian high variability index described in section 2. That is, we are looking at coherent upward WAF events occurring during surface conditions that are favored in high October SCE years. Figure 7a shows the climatological November–December eddy heights (zonal mean removed and scaled by the square root of density) for the latitude band 40°–80°N, and Fig. 7b shows the same eddy heights but composited only for those days when the upward WAF was positive and the SLP was high. The climatological eddy heights primarily reflect the jet-level, global wavenumber-2 pattern. During the upward WAF-high SLP events, the area of jet-level positive eddy heights between 0° and 60°E expands and extends down to the surface in western Siberia, with an overall westward tilt with height, consistent with the upward flux of negative momentum. As Fig. 7b illustrates, this feature is quite prominent in the entire hemispheric pattern—these are very large-scale events. The upward WAF–high SLP events occur twice as often during high October SCE years compared to low October SCE years, further establishing a close link between Eurasian snow cover and the resulting troposphere–stratosphere link.

Figure 8 is a reproduction of Fig. 7b but with the composite of standardized heights rather than the full field, thus illustrating the structure of the geopotential height field relative to its variance. This figure shows that the strongest signal occurs throughout the troposphere, highlighting the connection of the WAF–SLP events to lower-tropospheric processes. Hence, our analysis of geopotential heights for upward WAF–high SLP events shows a clear dynamical link through the troposphere between the surface and the lower stratosphere that is strongly related to antecedent snow

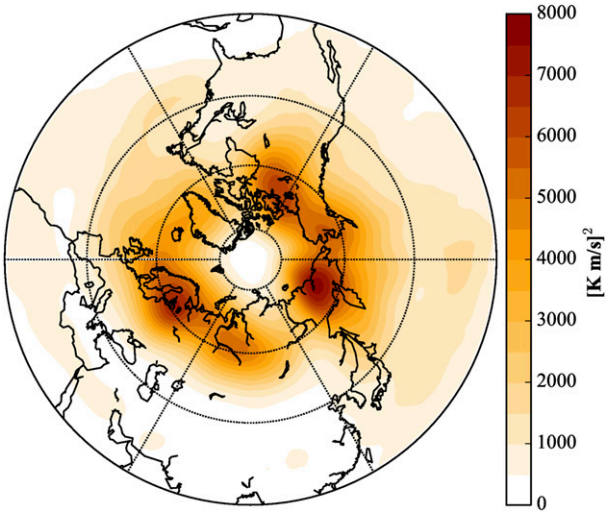

FIG. 6. Variance in daily December meridional heat flux anomalies $[(\mathrm{K\,m\,s^{-1}})^2]$ at 100 hPa.

conditions and is prominent in terms of the entire hemispheric pattern.

4. Conclusions

Previous studies by the authors and others established links between October Eurasian SCE variability and variability of the annular mode during the winter. However, a fundamental understanding of the long time lag (October–January) and the mechanism by which snow influences stratosphere–troposphere coupling has been lacking. The results presented in this article offer evidence of the immediate dynamical atmospheric response to snow cover variability, which further gives the novel result that both the near-surface and deep atmospheric responses have multiweek time scales far in excess of typical midlatitude values, suggesting the possibility of extratropical intraseasonal prediction.

The results presented in this study further support the six-step mechanism suggested by Cohen et al. (2007) between October Eurasian snow cover and the resulting boreal winter NH atmospheric variability. Observational analysis shows that high SCE in October across Eurasia favors the building of high SLP across northern Eurasia in the following six weeks from early November through mid-December (Figs. 3, 4, and 5a). Concomitantly, low pressure is favored in the northern Atlantic and Pacific Ocean basins forming a tripole SLP pattern that preferentially favors enhanced vertical wave propagation, particularly across eastern Eurasia and the North Pacific. With a two-week lag, poleward heat flux is enhanced in the lower stratosphere from mid-November through the end of December (Fig. 5b). Increased heat flux into the polar vortex over this time weakens the stratospheric polar vortex and may even cause a sudden stratospheric warming. The circulation anomalies associated with a stratospheric warming—high pressure over the pole, a weakening of the stratospheric westerly jet, and increased meridional flow—descend into the troposphere thereafter. These conditions are characteristic of the negative phase of the AO, high-latitude anticyclonic blocking, and an increased tendency toward severe winter weather across Eurasia and eastern North America.

The winter atmospheric circulation is driven by internal, external (e.g., solar, volcanoes) and coupled variability

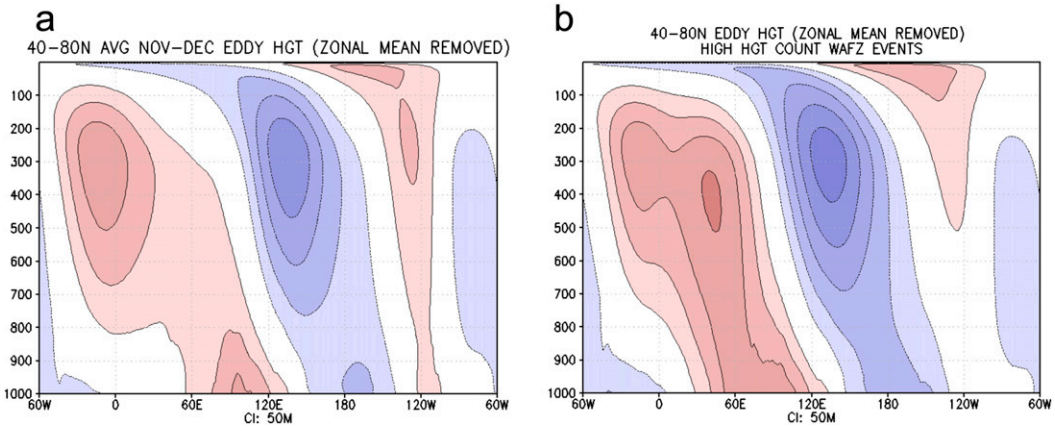

FIG. 7. (a) Climatological eddy height (m; zonal mean removed) averaged over 40°–80°N. (b) Eddy height (m) for high SLP poleward heat flux events over Siberia, averaged over 40°–80°N. The zonal mean has been removed but not the daily climatology; that is, this is the total geostrophic forcing of poleward heat flux. In (a) and (b) values are scaled by the square root of density and shaded every 50 m where red denotes positive values and blue denotes negative values.

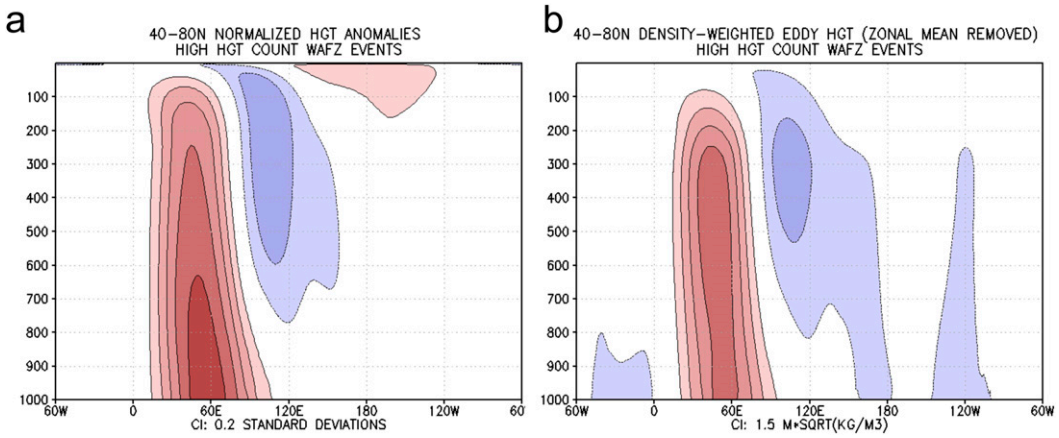

FIG. 8. (a) Daily normalized height anomalies for high SLP poleward heat flux events over Siberia. (b) As in (a), but values are scaled by the square root of density and averaged over 40°–80°N. Values are normalized and shaded every 0.2 standard deviations where red denotes positive values and blue denotes negative values. The full period daily mean was removed from each day prior to averaging, but the zonal mean is not removed. Each daily anomaly was divided by its standard deviation. Of the total number of days that compose this average, $^2/_3$ occur during high snow years and $^1/_3$ occur during low snow years.

with boundary conditions (e.g., tropical and extratropical sea surface temperatures, sea ice, and land surface hydrology). Our analysis has focused on just one boundary condition: terrestrial snow cover. The results presented suggest that a greater understanding of high-latitude land surface–atmosphere coupling may be exploited for improved boreal winter seasonal predictability and even longer-term climate change. Societal benefits from more accurate intraseasonal weather predictions are likely as governments and private entities can mitigate risk to anticipated severe winter weather. Also a better understanding of the feedback between a warming Arctic and more extreme weather will also educate society on the risks of longer-term climate change.

Three immediate avenues for future work exist from this study. One involves exploiting the intraseasonal (i.e., monthly) forecast benefits of this work. Recognition of the precursor patterns highlighted in this work (e.g., Figs. 3, 4, and 7b) offers opportunities to understand changes in storm tracks and vertical wave propagation, which may have implications for tropospheric conditions later. This recognition can also be used as a metric for assessing the performance of dynamical models used for intraseasonal and seasonal forecasts. Second, this work highlights how changes in surface land conditions (in this case, snow cover) impacts lower-tropospheric circulation patterns locally and remotely, and how these changes can extend throughout the troposphere. The current framework of snow–AO forcing may hold because the preferred tropospheric pattern constructively interferes with the climatological NH wave pattern (Fig. 4) and hence aids in enhancing vertical wave propagation (e.g., Smith and Kushner 2012). Sensitivity studies on the location and timing of snow cover advances may prove useful to understand further the coupling between the cryosphere and the atmosphere and those implications on weather and climate.

Third, observational studies can be used to diagnose dynamical models. Free running or control runs from GCMs in general lack the snow–AO relationship found in the observations (Hardiman et al. 2008; Riddle et al. 2013). However, models with forced or prescribed snow cover do simulate the observed snow–AO relationship (Gong et al. 2003; Fletcher et al. 2009; Peings et al. 2012). Furthermore Allen and Zender (2011) were able to simulate in a GCM recent decadal trends in the AO only when the model was forced with observed snow cover. Ongoing comparisons between modeling and observational studies will help us to better understand the robustness of the snow–AO relationship and ultimately will lead to advancements in model simulations of troposphere–stratosphere coupling that may include snow cover. Such improvements could potenitally lead to skillful model predictions of the AO, which currently do not exist (Hoskins 2013).

Acknowledgments. JC is supported by the National Science Foundation Grants BCS-1060323 and AGS-1303647 and NOAA Grant NA10OAR4310163.

REFERENCES

Allen, R. J., and C. S. Zender, 2011: Forcing of the Arctic Oscillation by Eurasian snow cover. *J. Climate,* **24,** 6528–6539, doi:10.1175/2011JCLI4157.1.

Baldwin, M. P., and T. J. Dunkerton, 1999: Propagation of the Arctic Oscillation from the stratosphere to the troposphere. *J. Geophys. Res.,* **104,** 30 937–30 946, doi:10.1029/1999JD900445.

——, and ——, 2001: Stratospheric harbingers of anomalous weather regimes. *Science,* **294,** 581–584, doi:10.1126/science.1063315.

Charney, J. G., and P. G. Drazin, 1961: Propagation of planetary-scale disturbances from the lower into the upper atmosphere. *J. Geophys. Res.,* **66,** 83–109, doi:10.1029/JZ066i001p00083.

Christiansen, B., 2003: Evidence for nonlinear climate change: Two stratospheric regimes and a regime shift. *J. Climate,* **16,** 3681–3689, doi:10.1175/1520-0442(2003)016<3681:EFNCCT>2.0.CO;2.

——, 2005: Downward propagation and statistical forecast of the near-surface weather. *J. Geophys. Res.,* **110,** D14104, doi:10.1029/2004JD005431.

Cohen, J., and D. Entekhabi, 1999: Eurasian snow cover variability and Northern Hemisphere climate predictability. *Geophys. Res. Lett.,* **26,** 345–348, doi:10.1029/1998GL900321.

——, and C. Fletcher, 2007: Improved skill for Northern Hemisphere winter surface temperature predictions based on land–atmosphere fall anomalies. *J. Climate,* **20,** 4118–4132, doi:10.1175/JCLI4241.1.

——, and J. Jones, 2011a: A new index for more accurate winter predictions. *Geophys. Res. Lett.,* **38,** L21701, doi:10.1029/2011GL049626.

——, and ——, 2011b: Tropospheric precursors and stratospheric warmings. *J. Climate,* **24,** 6562–6572, doi:10.1175/2011JCLI4160.1.

——, A. Frei, and R. Rosen, 2005: Evaluation of the role of boundary conditions in AMIP-2 simulations of the NAO. *J. Climate,* **18,** 973–981, doi:10.1175/JCLI-3305.1.

——, M. Barlow, P. Kushner, and K. Saito, 2007: Stratosphere–troposphere coupling and links with Eurasian land surface variability. *J. Climate,* **20,** 5335–5343, doi:10.1175/2007JCLI1725.1.

Delsole, T., and J. Shukla, 2006: Specification of wintertime North American surface temperature. *J. Climate,* **19,** 2691–2716, doi:10.1175/JCLI3704.1.

Eliassen, A., and E. Palm, 1961: On the transfer of energy in stationary mountain waves. *Geophys. Publ.,* **22,** 1–23.

Feldstein, S. B., 2002: The recent trend and variance increase of the annular mode. *J. Climate,* **15,** 88–94, doi:10.1175/1520-0442(2002)015<0088:TRTAVI>2.0.CO;2.

Fletcher, C., S. C. Hardiman, P. J. Kushner, and J. Cohen, 2009: The dynamical response to snow cover perturbations in a large ensemble of atmospheric GCM integrations. *J. Climate,* **22,** 1208–1222, doi:10.1175/2008JCLI2505.1.

Folland, C. K., A. A. Scaife, J. Lindesay, and D. B. Stephenson, 2012: How potentially predictable is northern European winter climate a season ahead? *Int. J. Climatol.,* **32,** 801–818, doi:10.1002/joc.2314.

Garfinkel, C. I., D. L. Hartmann, and F. Sassi, 2010: Tropospheric precursors of anomalous Northern Hemisphere stratospheric polar vortices. *J. Climate,* **23,** 3282–3299, doi:10.1175/2010JCLI3010.1.

Gong, G., D. Entekhabi, and J. Cohen, 2003: Modeled Northern Hemisphere winter climate response to realistic Siberian snow anomalies. *J. Climate,* **16,** 3917–3931, doi:10.1175/1520-0442(2003)016<3917:MNHWCR>2.0.CO;2.

Hardiman, S. C., P. J. Kushner, and J. Cohen, 2008: Investigating the ability of general circulation models to capture the effects of Eurasian snow cover on winter climate. *J. Geophys. Res.,* **113,** D21123, doi:10.1029/2008JD010623.

Honda, M., J. Inue, and S. Yamane, 2009: Influence of low Arctic sea-ice minima on anomalously cold Eurasian winters. *Geophys. Res. Lett.,* **36,** L08707, doi:10.1029/2008GL037079.

Hoskins, B., 2013: The potential for skill across the range of the seamless weather-climate prediction problem: A stimulus for our science. *Quart. J. Roy. Meteor. Soc.,* **139,** 573–584, doi:10.1002/qj.1991.

Ineson, S., and A. A. Scaife, 2009: The role of the stratosphere in the European climate response to El Niño. *Nat. Geosci.,* **2,** 32–36, doi:10.1038/ngeo381.

Joshi, M. M., A. J. Charlton, and A. A. Scaife, 2006: On the influence of stratospheric water vapor changes on the tropospheric circulation. *Geophys. Res. Lett.,* **33,** L09806, doi:10.1029/2006GL025983.

Keeley, S. P. E., R. T. Sutton, and L. C. Shaffrey, 2009: Does the North Atlantic Oscillation show unusual persistence on intraseasonal timescales? *Geophys. Res. Lett.,* **36,** L22706, doi:10.1029/2009GL040367.

Kim, H.-M., P. J. Webster, and J. A. Curry, 2012: Seasonal prediction skill of ECMWF System 4 and NCEP CFSv2 retrospective forecast for the Northern Hemisphere Winter. *Climate Dyn.,* **39,** 2957–2973, doi:10.1007/s00382-012-1364-6.

Kolstad, E. W., and A. J. Charlton-Perez, 2011: Observed and simulated precursors of stratospheric polar vortex anomalies in the Northern Hemisphere. *Climate Dyn.,* **37,** 1443–1456, doi:10.1007/s00382-010-0919-7.

——, T. Breiteig, and A. A. Scaife, 2010: The association between stratospheric weak polar vortex events and cold air outbreaks in the Northern Hemisphere. *Quart. J. Roy. Meteor. Soc.,* **136,** 886–893, doi:10.1002/qj.620.

Kumar, A., B. Jha, Q. Zhang, and L. Bounoua, 2007: A new methodology for estimating the unpredictable component of seasonal atmospheric variability. *J. Climate,* **20,** 3888–3901, doi:10.1175/JCLI4216.1.

Liu, J., J. A. Curry, and Y. Y. Hu, 2004: Recent Arctic sea ice variability: Connections to the Arctic Oscillation and the ENSO. *Geophys. Res. Lett.,* **31,** L09211, doi:10.1029/2004GL019858.

——, ——, H. Wang, M. Song, and R. Horton, 2012: Impact of declining Arctic sea ice on winter snowfall. *Proc. Natl. Acad. Sci.,* **109,** 4074–4079, doi:10.1073/pnas.1114910109.

Madden, R. A., and P. R. Julian, 1994: Observations of the 40–50 day tropical oscillation: A review. *Mon. Wea. Rev.,* **122,** 814–837, doi:10.1175/1520-0493(1994)122<0814:OOTDTO>2.0.CO;2.

Marshall, A. G., A. A. Scaife, and S. Ineson, 2009: Enhanced seasonal prediction of European winter warming following volcanic eruptions. *J. Climate,* **22,** 6168–6180, doi:10.1175/2009JCLI3145.1.

Matsuno, T., 1970: Vertical propagation of stationary planetary waves in the winter Northern Hemisphere. *J. Atmos. Sci.,* **27,** 871–883, doi:10.1175/1520-0469(1970)027<0871:VPOSPW>2.0.CO;2.

Pascoe, C. L., L. J. Gray, and A. A. Scaife, 2006: A GCM study of the influence of equatorial winds on the timing of sudden stratospheric warmings. *Geophys. Res. Lett.,* **33,** L06825, doi:10.1029/2005GL024715.

Peings, Y., D. Saint-Martin, and H. Douville, 2012: A numerical sensitivity study of the influence of Siberian snow on the northern annular mode. *J. Climate,* **25,** 592–607, doi:10.1175/JCLI-D-11-00038.1.

——, E. Brun, V. Mauvais, and H. Douville, 2013: How stationary is the relationship between Siberian snow and Arctic Oscillation over the 20th century? *Geophys. Res. Lett.,* **40,** 183–188, doi:10.1029/2012GL054083.

Plumb, R. A., 1985: On the three-dimensional propagation of stationary waves. *J. Atmos. Sci.,* **42,** 217–229, doi:10.1175/1520-0469(1985)042<0217:OTTDPO>2.0.CO;2.

Polvani, L. M., and D. W. Waugh, 2004: Upward wave activity flux as precursor to extreme stratospheric events and subsequent anomalous surface weather regimes. *J. Climate,* **17,** 3548–3554, doi:10.1175/1520-0442(2004)017<3548:UWAFAA>2.0.CO;2.

Quan, X., M. Hoerling, J. Whitaker, G. Bates, and T. Xu, 2006: Diagnosing sources of U.S. seasonal forecast skill. *J. Climate,* **19,** 3279–3293, doi:10.1175/JCLI3789.1.

Rasmusson, E. M., and T. H. Carpenter, 1982: Variations in tropical sea surface temperature and surface wind fields associated with the Southern Oscillation/El Niño. *Mon. Wea. Rev.,* **110,** 354–384, doi:10.1175/1520-0493(1982)110<0354:VITSST>2.0.CO;2.

Riddle, E. E., A. H. Butler, J. C. Furtado, J. L. Cohen, and A. Kumar, 2013: CFSv2 ensemble prediction of the wintertime Arctic Oscillation. *Climate Dyn.,* **41,** 1099–1116, doi:10.1007/s00382-013-1850-5.

Rienecker, M. M., and Coauthors, 2011: MERRA: NASA's Modern-Era Retrospective Analysis for Research and Applications. *J. Climate,* **24,** 3624–364, doi:10.1175/JCLI-D-11-00015.1.

Robinson, D. A., F. Dewey, and R. Heim Jr., 1993: Northern Hemispheric snow cover: An update. *Bull. Amer. Meteor. Soc.,* **74,** 1689–1696, doi:10.1175/1520-0477(1993)074<1689:GSCMAU>2.0.CO;2.

Saha, S., and Coauthors, 2006: The NCEP Climate Forecast System. *J. Climate,* **19,** 3483–3517, doi:10.1175/JCLI3812.1.

Smith, K. L., and P. J. Kushner, 2012: Linear interference and the initiation of extratropical stratosphere–troposphere interactions. *J. Geophys. Res.,* **117,** D13107, doi:10.1029/2012JD017587.

——, ——, and J. Cohen, 2011: The role of linear interference in northern annular mode variability associated with Eurasian snow cover extent. *J. Climate,* **24,** 6185–6202, doi:10.1175/JCLI-D-11-00055.1.

Stenchikov, G., K. Hamilton, R. J. Stouffer, A. Robock, V. Ramaswamy, B. Santer, and H.-F. Graf, 2006: Arctic Oscillation response to volcanic eruptions in the IPCC AR4 climate models. *J. Geophys. Res.,* **111,** D07107, doi:10.1029/2005JD006286.

Thompson, D. W. J., and J. M. Wallace, 1998: The Arctic Oscillation signature in the wintertime geopotential height and temperature fields. *Geophys. Res. Lett.,* **25,** 1297–1300, doi:10.1029/98GL00950.

——, and ——, 2001: Regional climate impacts of the Northern Hemisphere annular mode. *Science,* **293,** 85–89, doi:10.1126/science.1058958.